

Lifshitz transition in triangular lattice Kondo-Heisenberg model

Lan Zhang(张欄), Yin Zhong(钟寅), Hong-Gang Luo(罗洪刚)

Citation: Chin. Phys. B . 2020, 29(7): 077102 . **doi:** 10.1088/1674-1056/ab8da4
Journal homepage: http://cpb.iphy.ac.cn; http://iopscience.iop.org/cpb

What follows is a list of articles you may be interested in

Point-contact spectroscopy on antiferromagnetic Kondo semiconductors CeT_2Al$_{10}$ (T=Ru and Os)

Jie Li(李洁), Li-Qiang Che(车利强), Tian Le(乐天), Jia-Hao Zhang(张佳浩), Pei-Jie Sun(孙培杰), Toshiro Takabatake, Xin Lu(路欣)

Chin. Phys. B . 2020, 29(7): 077103 . **doi:** 10.1088/1674-1056/ab8dab

Giant topological Hall effect of ferromagnetic kagome metal Fe_3Sn_2

Qi Wang(王琦), Qiangwei Yin(殷蔷薇), Hechang Lei(雷和畅)

Chin. Phys. B . 2020, 29(1): 017101 . **doi:** 10.1088/1674-1056/ab5fbc

Possible nodeless $s^{\pm}$-wave superconductivity in twisted bilayer graphene

Zhe Liu(刘哲), Yu Li(李宇), Yi-Feng Yang(杨义峰)

Chin. Phys. B . 2019, 28(7): 077103 . **doi:** 10.1088/1674-1056/28/7/077103

Negative differential resistance and quantum oscillations in $FeSb_2$ with embedded antimony

Fangdong Tang(汤方栋), Qianheng Du(杜乾衡), Cedomir Petrovic, Wei Zhang(张威), Mingquan He(何明全), Liyuan Zhang(张立源)

Chin. Phys. B . 2019, 28(3): 037104 . **doi:** 10.1088/1674-1056/28/3/037104

Magnetochemistry and chemical synthesis

Lin Hu(胡林), Guoliang Xia(夏国良), Qianwang Chen(陈乾旺)

Chin. Phys. B . 2019, 28(3): 037102 . **doi:** 10.1088/1674-1056/28/3/037102

Lifshitz transition in triangular lattice Kondo–Heisenberg model*

Lan Zhang(张欄)[1], Yin Zhong(钟寅)[1,†], and Hong-Gang Luo(罗洪刚)[1,2]

[1] School of Physical Science and Technology & Key Laboratory for Magnetism and Magnetic Materials of Ministry of Education, Lanzhou University, Lanzhou 730000, China

[2] Beijing Computational Science Research Center, Beijing 100084, China

(Received 3 March 2020; revised manuscript received 23 April 2020; accepted manuscript online 28 April 2020)

Motivated by recent experimental progress on triangular lattice heavy-fermion compounds, we investigate possible Lifshitz transitions and the scanning tunnel microscope (STM) spectra of the Kondo–Heisenberg model on the triangular lattice. In the heavy Fermi liquid state, the introduced Heisenberg antiferromagnetic interaction ($J_{\rm H}$) results in the twice Lifshitz transition at the case of the nearest-neighbour electron hopping but with next-nearest-neighbour hole hopping and the case of the nearest-neighbour hole hopping but with next-nearest-neighbour electron hopping, respectively. Driven by $J_{\rm H}$, the Lifshitz transitions on triangular lattice are all continuous in contrast to the case on square lattice. Furthermore, the STM spectra shows rich line-shape which is influenced by the Kondo coupling $J_{\rm K}$, the Heisenberg antiferromagnetic interaction $J_{\rm H}$, and the ratio of the tunneling amplitude of f-electron $t_{\rm f}$ versus conduction electron $t_{\rm c}$. Our work provides a possible scenario to understand the Fermi surface topology and the quantum critical point in heavy-fermion compounds.

Keywords: Kondo–Heisenberg model, Lifshitz transition, heavy-fermion systems

PACS: 71.27.+a, 71.18.+y **DOI:** 10.1088/1674-1056/ab8da4

1. Introduction

The Lifshitz transition, where the Fermi surface (FS) topology changes,[1] is beyond the paradigm of Landau's symmetry breaking theory. This unconventional transition has been observed experimentally in cuprate superconductors,[2–4] iron-based superconductors,[5–13] topological insulator,[14] graphene,[15] and heavy-fermion compounds.[16–21] Particularly, for some quantum critical heavy-fermion materials, such as $YbRh_2Si_2$, its magnetic field dependent thermopower, thermal conductivity, resistivity, and Hall effect show three transitions at high fields and the Lifshitz transitions are argued to be their origin.[20] For $CeRu_2Si_2$, the high resolution Hall effect and magnetoresistance measurements across the metamagnetic transition are explained as an abrupt f-electron localization, where one of the spin-split sheets of the heaviest Fermi surface shrinks to a point.[16] The Lifshitz transition leads to a way to understand the relation of the FS topology and the quantum critical point in heavy-fermion systems.[22]

Theoretically, the Lifshitz transitions in heavy fermion systems have been carefully explored with mean-field theory and dynamical mean-field theory.[23–34] At the mean-field level, the Lifshitz transition is triggered with the introduction of Heisenberg coupling into the usual Kondo lattice model, i.e., Kondo–Heisenberg model (KHM), and a case studying on square lattice suggests both first and second-order Lifshitz transitions.[23–25] Interestingly, the appearance of Lifshitz transition with enhanced antiferromagnetic Heisenberg interaction preempts the disentanglement of Kondo singlet, thus the resulting Kondo breakdown mechanism predicted in literature should be reexamined.[26,35,36]

Recently, non-Fermi liquid behaviors have been observed in triangular lattice heavy-fermion compounds like YbAgGe and $YbAl_3C_3$.[37–42] Due to the frustration effect introduced by local f-electron spin located on the triangular lattice, the observed non-Fermi liquid phenomena could be linked to the idea of Kondo breakdown, where critical Kondo boson and deconfined gauge field induce singularity in thermodynamics and transport.[37,39,42] However, as exemplified by the study on the square lattice, the topology of FS may change radically before any noticeable breakdown of the Kondo effect, therefore the possibility of Lifshitz transition on triangular lattice should be investigated first.

In the present work, we employ the large-N mean-field approach to study the KHM on the triangular lattice. As expected, we find that the Heisenberg antiferromagnetic interaction ($J_{\rm H}$) induces twice FS topology changes at the case of the nearest-neighbour (NN) electron hopping but with next-nearest-neighbour (NNN) hole hopping and the case of the NN hole hopping but with NNN electron hopping. Both Lifshitz transitions are continuous. The density of state (DOS) of the conduction electron is changed by $J_{\rm H}$. To meet with experiments, we give the STM line-shape of the differential conductance $\mathrm{d}I/\mathrm{d}V$ for different Kondo coupling ($J_{\rm K}$) and the ratio of the tunneling amplitude of f-electron $t_{\rm f}$ versus conduction

*Project supported by the National Natural Science Foundation of China (Grant Nos. 11674139, 11704166, and 11834005), the Fundamental Research Funds for the Central Universities, China, and PCSIRT, China (Grant No. IRT-16R35).

†Corresponding author. E-mail: zhongy@lzu.edu.cn

© 2020 Chinese Physical Society and IOP Publishing Ltd

electron t_c. The calculated spectra are qualitatively consistent with data of $CeCoIn_5$.[43]

Compared with the square lattice KHM, the triangular lattice KHM also has the Lifshitz transition, which is driven by the Heisenberg coupling J_H. The energy spectrum local maximum values of the triangular lattice and the square lattice KHM both move towards $M \to \Gamma$ at the case of the NN electron hopping but with NNN hole hopping. However, the triangular lattice has a continuous quantum phase transition around the Lifshitz transition points, while the square lattice has the first-order and second-order phase transitions.[23] As changes of FS topology can be reflected in the effective mass, the effective mass enhancement $m^\star/m$ of the triangular lattice is smooth, leading to the continuous quantum phase transition around the Lifshitz transition, which is different from the square lattice in which $m^\star/m$ has the singularity at the Lifshitz transition points.[23]

The paper is organized as follows. In Section 2, we describe the Kondo–Heisenberg model under the large-N mean-field theory. In Section 3, we present the Lifshitz transition and the DOS of conduction electron. In Section 4, we give the line-shape of differential conductance at different Heisenberg antiferromagnetic interaction, the Kondo coupling, and the ratio of the tunneling amplitude of f-electron to conduction electron. Finally, Section 5 is devoted to a brief conclusion and perspective.

2. Model and mean-field approach

The basic structure and the first Brillouin zone are shown in Fig. 1. The model Hamiltonian of the KHM is given by

$$\begin{aligned} H =& -t\sum_{\langle ij\rangle\sigma} c^\dagger_{i\sigma}c_{j\sigma} + t_1\sum_{\langle\langle ij\rangle\rangle\sigma} c^\dagger_{i\sigma}c_{j\sigma} - \mu\sum_{i\sigma} c^\dagger_{i\sigma}c_{i\sigma} \\ &+ J_K\sum_i \boldsymbol{S}_i\cdot\boldsymbol{s}_i + J_H\sum_{\langle ij\rangle}\boldsymbol{S}_i\cdot\boldsymbol{S}_j, \end{aligned} \tag{1}$$

where $c^\dagger_{i\sigma}$ ($c_{i\sigma}$) denotes the creation (annihilation) operator of conduction electron with spin $\sigma =\uparrow,\downarrow$. The first line in Eq. (1) describes the hoppings of conduction electron and μ is the chemical potential. $\langle\cdot\rangle$ and $\langle\langle\cdot\rangle\rangle$ represent the NN and the NNN hoppings, respectively (The NNN hopping is introduced to avoid the occasional nesting). The J_K term in the second line denotes the Kondo coupling between the localized f-electron and conduction electron. $\boldsymbol{S}_i = \frac{1}{2}\sum_{\alpha\beta} f^\dagger_{i\alpha}\tau_{\alpha\beta}f_{i\beta}$ is the fermionic representation of localized f-electron spin with the local constraint $\sum_\sigma f^\dagger_{i\sigma}f_{i\sigma} = 1$, while $\boldsymbol{s}_i = \frac{1}{2}\sum_{\sigma\sigma'} c^\dagger_{i,\sigma}\tau_{\sigma\sigma'}c_{i,\sigma'}$ is for conduction electron. The last J_H term is the Heisenberg exchange interaction firstly introduced by Coleman and Andrei.[44] It has also been used by Iglesias *et al.* to consider the antiferromagnetic long-range order in some Ce-based heavy fermion compounds.[45–47]

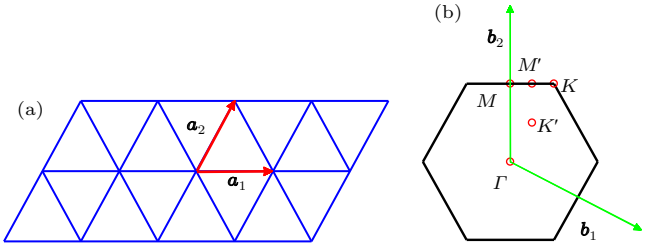


Fig. 1. (a) The real space triangular lattice, $\boldsymbol{a}_1 = (0,a)$ and $\boldsymbol{a}_2 = \left(\frac{a}{2}, \frac{\sqrt{3}a}{2}\right)$ are the basic vectors. (b) The first Brillouin zone of the triangular lattice, $\boldsymbol{b}_1 = (2\pi, \frac{2\pi}{\sqrt{3}})$ and $\boldsymbol{b}_2 = \left(0, \frac{4\pi}{\sqrt{3}}\right)$ are the reciprocal vectors of the triangular lattice, the red dots are high symmetry points of the first Brillouin zone, where $\Gamma = (0,0)$, $K = \left(\frac{2\pi}{3}, \frac{2\pi}{\sqrt{3}}\right)$, $M = \left(0, \frac{2\pi}{\sqrt{3}}\right)$, $K' = \left(\frac{\pi}{3}, \frac{\pi}{\sqrt{3}}\right)$, $M' = \left(\frac{\pi}{3}, \frac{2\pi}{\sqrt{3}}\right)$.

To proceed, we use the fermionic large-N mean-field method,[48] which is believed to capture qualitative features in heavy Fermi liquid states. Introducing valence-bond order parameter $\chi_{ij} = -\left\langle \Sigma_\alpha f^\dagger_{i\alpha}f_{j\alpha}\right\rangle$ and Kondo hybridization parameter $V_i = \left\langle \Sigma_\alpha f^\dagger_{i,\alpha}c_{i\alpha}\right\rangle$,[23] and further considering the uniform resonance-valence-bond ansatz $\chi_{ij} = \chi$ and the uniform Kondo hybridization $V_i = V$, as done in Refs. [23,49], one can obtain $\boldsymbol{S}_i\cdot\boldsymbol{S}_j = \frac{1}{2}\left[\chi(f^\dagger_{i\uparrow}f_{j\uparrow} + f^\dagger_{i\downarrow}f_{j\downarrow}) + \text{H.c.}\right] + \frac{\chi^2}{2}$. Based on these mean-field formulations, equation (1) can be rewritten in the k-space as follows:

$$\begin{aligned} H =& \sum_k \Psi^\dagger_k \begin{pmatrix} \varepsilon_k - \mu & -\frac{J_K V}{2} \\ -\frac{J_K V}{2} & \chi_k \end{pmatrix} \Psi_k + \sum_{k\sigma}\chi_k f^\dagger_{k\sigma}f_{k\sigma} \\ &+ N_S\left(\frac{J_K V^2}{2} + \frac{3J_H\chi^2}{2} - \lambda\right), \end{aligned} \tag{2}$$

where $\Psi^\dagger_{\boldsymbol{k}} = \left(c^\dagger_{\boldsymbol{k}\sigma}, f^\dagger_{\boldsymbol{k}\sigma}\right)$ is a two-component Nambu spinor, $\gamma_k = 2\cos(\sqrt{3}k_y/2)\cos(k_x/2) + \cos(k_x)$, $\chi_k = J_H\chi\gamma_k + \lambda$ is the kinetic energy of the f-electron, and $\varepsilon_k = 2t_1[2\cos(\sqrt{3}k_y/2)\cos(3k_x/2) + \cos(\sqrt{3}k_y)] - 2t\gamma_k$ denotes the energy spectrum of conduction electron. Also, the Lagrangian multiplier λ is introduced to impose the local constraint on average. The quasiparticle excitation spectra can be easily obtained by

$$E^\pm_k = \frac{(\varepsilon_k - \mu + \chi_k)}{2} \pm \frac{\sqrt{(\varepsilon_k - \mu - \chi_k)^2 + J_K^2V^2}}{2}. \tag{3}$$

The ground-state energy of the KHM is

$$E_g = \frac{2}{N_S}\sum_{k,\pm} E^\pm_k\theta(-E^\pm_k) + \left(\frac{J_K V^2}{2} + \frac{3J_H\chi^2}{2} - \lambda\right), \tag{4}$$

where $\theta(x)$ is the step function. The factor 2 comes from the spin degeneracy. Then, the MF equations for χ, V, λ can be derived by minimizing the ground-state energy and the chemical potential μ is determined by the conduction electron density n_c, i.e., $\partial E_g/\partial\chi = 0$, $\partial E_g/\partial V = 0$, $\partial E_g/\partial\lambda = 0$,

$-\partial E_g/\partial\mu = n_c$. One can obtain four self-consistent MF equations

$$-\frac{1}{N_S}\sum_{k,\pm}\theta(-E_k^{\pm})\gamma_k\left[1\mp\frac{(\varepsilon_k-\mu-\chi_k)}{W_k}\right]=3\chi, \quad (5)$$

$$-\frac{1}{N_S}\sum_{k,\pm}\theta(-E_k^{\pm})\left[\frac{\pm J_K}{W_k}\right]=1, \quad (6)$$

$$\frac{1}{N_S}\sum_{k,\pm}\theta(-E_k^{\pm})\left[1\mp\frac{(\varepsilon_k-\mu-\chi_k)}{W_k}\right]=1, \quad (7)$$

$$\frac{1}{N_S}\sum_{k,\pm}\theta(-E_k^{\pm})\left[1\pm\frac{(\varepsilon_k-\mu-\chi_k)}{W_k}\right]=n_c, \quad (8)$$

where $W_k=\sqrt{(\varepsilon_k-\mu-\chi_k)^2+(J_K V)^2}$.

3. Lifshitz transition

We consider the case of $J_H \ll J_K$, where the paramagnetic heavy Fermi liquid state is stable compared to other symmetry-breaking and exotic fractionalized states. When the Heisenberg interaction J_H increases, the band structure of quasiparticle evolves and a Lifshitz transition is expected to occur.

The FS is a normal circle when J_H is small as shown in Figs. 2(a) and 3(a), which means the influence of the short-range antiferromagntic correlation is negligible. Our system has twice Lifshitz transitions in two cases as shown in Figs. 2(d), 2(e), 3(b), and 3(e). In Figs. 2(d) and 3(b), there emerges a small circle below FS at the center, the quasiparticles begin to fill the area between the two loops. In Figs. 2(e) and 3(e), the FS happens to split into many Fermi pockets after this critical point, each pocket is the FS of hole quasiparticle. The Lifshitz quantum critical point for NN electron hopping with NNN hole hopping has the larger Heisenberg coupling J_H than the case of the NN hole hopping with NNN electron hopping.

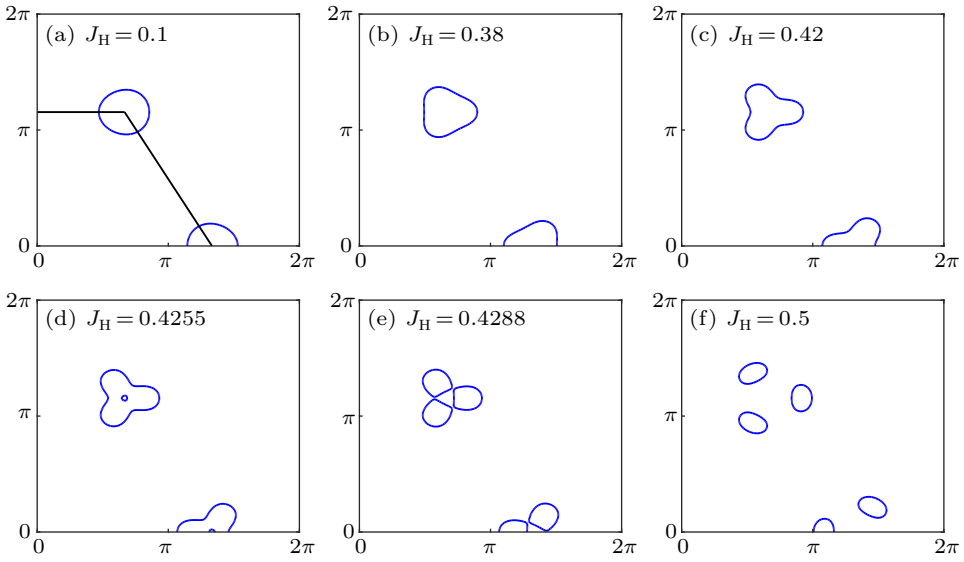


Fig. 2. The FS evolution of the KHM versus the Heisenberg interaction J_H for NN electron hopping but with NNN hole hopping, the first Brillouin zone of the triangular lattice is marked by the black line, where the parameters are $t=1$, $t_1/t=0.3$, $n_c=0.9$, $J_K=2.5$.

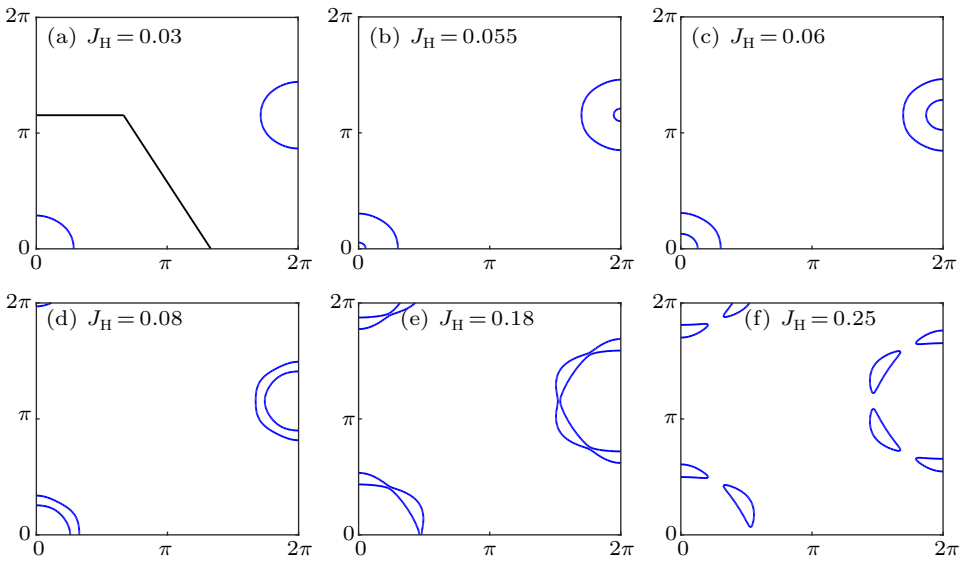


Fig. 3. The FS evolution of the KHM versus the Heisenberg interaction J_H for NN hole hopping but with NNN electron hopping, the first Brillouin zone of the triangular lattice is marked by the black line, where the parameters are $t=-1$, $t_1/t=0.3$, $n_c=0.9$, $J_K=2.5$.

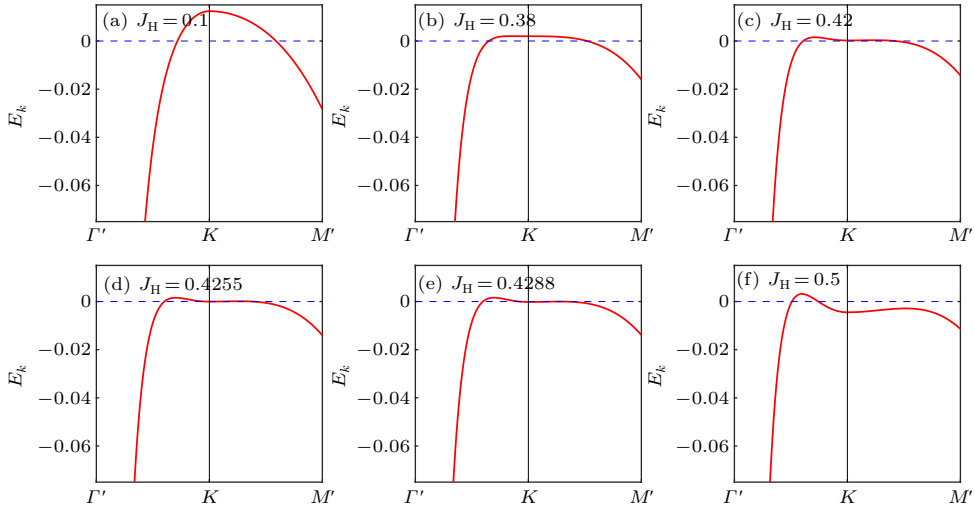


Fig. 4. The quasiparticle energy spectra of the KHM from the direction $\Gamma'\left(\frac{\pi}{3},\frac{\pi}{\sqrt{3}}\right)\rightarrow K\left(\frac{2\pi}{3},\frac{2\pi}{\sqrt{3}}\right)\rightarrow M'\left(\frac{\pi}{3},\frac{2\pi}{\sqrt{3}}\right)$ for NN electron hopping but with NNN hole hopping, the blue dashed line denotes the Fermi energy level, where the parameters are $t=1$, $t_1/t=0.3$, $n_{\rm c}=0.9$, $J_{\rm K}=2.5$.

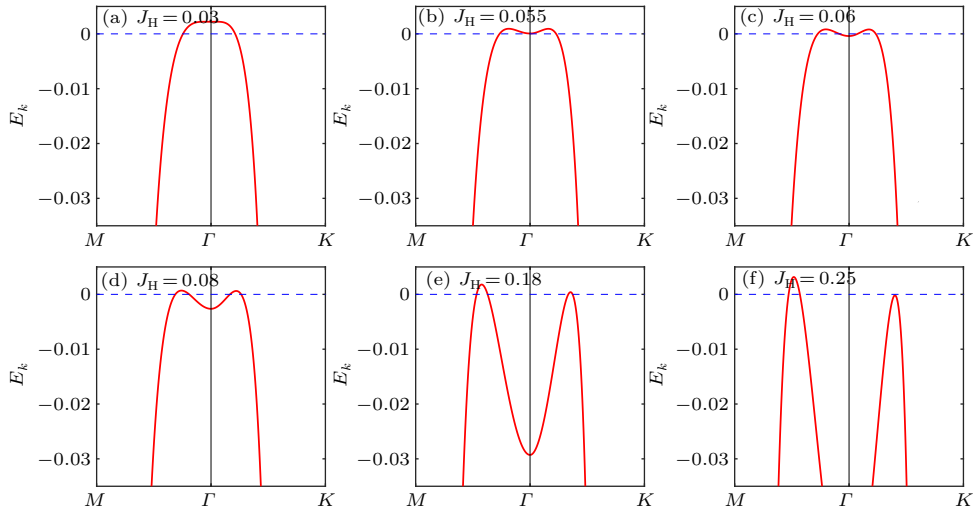


Fig. 5. The quasiparticle energy spectra of the KHM from the direction $M\left(0,\frac{2\pi}{\sqrt{3}}\right)\rightarrow\Gamma\,(0,0)\rightarrow K\left(\frac{2\pi}{3},\frac{2\pi}{\sqrt{3}}\right)$ for NN hole hopping but with NNN electron hopping, the blue dashed line denotes the Fermi energy level, where the parameters are $t=-1$, $t_1/t=0.3$, $n_{\rm c}=0.9$, $J_{\rm K}=2.5$.

We also give the quasiparticle energy spectra of these two cases to interpret the FS topology change as shown in Figs. 4 and 5. When $J_{\rm H}$ is increasing, the short-range antiferromagnetic correlation starts to change the electronic structure, and the FS begins to deform. In Figs. 4(a) and 4(b), the energy spectrum shows one local maximum across the Fermi energy around the K point, which gives the hole quasiparticle FS as shown in Figs. 2(a) and 4(b). When $J_{\rm H}>0.38$, there are two local maxima as shown in Figs. 4(c)–4(f) and 2(c)–2(f). In Fig. 5(a), the energy spectrum has one local maximum across the Fermi energy around the Γ point, which has the FS as shown in Fig. 3(a). When $0.055<J_{\rm H}<0.18$, there are two local maxima across the Fermi energy, which induces the hole quasiparticle occupation among two FSs as shown in Figs. 5(b)–5(e) and 3(b)–2(e). When $J_{\rm H}>0.18$, the maximum just crosses the Fermi energy as shown in Figs. 5(f) and 3(f). The FS moves towards $M\rightarrow\Gamma$ versus the Heisenberg coupling $J_{\rm H}$ at the case of NN electron hopping but with NNN hole hopping as shown in Figs. 2 and 4, in contrast to $\Gamma\rightarrow M$ in the case of NN hole hopping but with NNN electron hopping as shown in Figs. 3 and 5.

According to many experiments on heavy-fermion quantum critical compounds $YbRh_2Si_2$ and $CeRu_2Si_2$,[16,20] the FS change is related to the quantum phase transition. Thus, to identify the quantum phase transition around the Lifshitz transition, the ground-state energy $E_{\rm g}$ and its first-order derivative $\mathrm{d}E_{\rm g}/\mathrm{d}J_{\rm H}$ versus $J_{\rm H}$ are shown in Figs. 6 and 7, where $\mathrm{d}E_{\rm g}/\mathrm{d}J_{\rm H}$ is given by

$$\frac{\mathrm{d}E_{\rm g}}{\mathrm{d}J_{\rm H}}=\frac{1}{N_{\rm S}}\sum_{k,\pm}\theta(-E_k^{\pm})\chi\gamma_k\left[1\mp\frac{(\varepsilon_k-\mu-\chi_k)}{W_k}\right]+\frac{3\chi^2}{2}. \quad (9)$$

Both lines are smooth across the changes of FS topology, which demonstrates that the Lifshitz transitions are not the second-order quantum phase transition, but belong to the

higher-order continuous phase transitions. In order to interpret this continuous phase transition, we give the effective mass of the heavy quasiparticle excitations, which is a function of the band curvature, and the topological changes of the FS can be reflected in the effective mass.[23] This is given by[23]

$$\frac{m}{m^{\star}} = \left\langle \frac{\partial E_k^-}{\partial \varepsilon_k} \right\rangle_{\rm FS} = \frac{1}{N_{\rm S}} \sum_k \left[\frac{\partial E_k^-}{\partial \varepsilon_k} \right] \delta(\mu - \varepsilon_k). \tag{10}$$

We can obtain effective mass enhancement $m^{\star}/m$ at these two cases as shown in Fig. 8. The effective mass enhancement $m^{\star}/m$ is increasing versus the Heisenberg coupling $J_{\rm H}$ at the case of NN electron hopping but with NNN hole hopping, while the effective mass enhancement $m^{\star}/m$ is decreasing versus the Heisenberg coupling $J_{\rm H}$ at the case of NN hole hopping but with NNN electron hopping. However, both lines are smooth versus the Heisenberg coupling $J_{\rm H}$, which implies that the triangular lattice Lifshitz transitions are continuous quantum phase transitions because of the smooth effective mass enhancement. This is different from the case in the square lattice in which the effective mass enhancement $m^{\star}/m$ has the singularity at the Lifshitz transition points.[23]

The DOS of the conduction electron is shown in Figs. 9 and 10. The Heisenberg interaction $J_{\rm H}$ has an effect on the DOS of the conduction electron $\rho_{\rm c}$, the larger $J_{\rm H}$ induces the larger gap. Thus, the DOS is changed after the Lifshitz transition. In Figs. 9(a) and 9(b), the DOS has a gap and two peaks. At $J_{\rm H} = 0.4255$, it develops a new small peak as shown in Fig. 9(c). The conduction electron DOS has one gap and three peaks when $J_{\rm H} > 0.4255$ as shown in Figs. 9(c)–9(f). In Fig. 10, the DOS always has a gap and two peaks, but the left peak is lower than the right peak in Figs. 10(a)–10(d), while becomes higher than the right peak in Figs. 10(e) and 10(f). Both peaks are increasing versus the Heisenberg coupling $J_{\rm H}$, and the peak at $\omega < 0$ arises from the van Hove singularity of the large (hybridized) FS.[50]

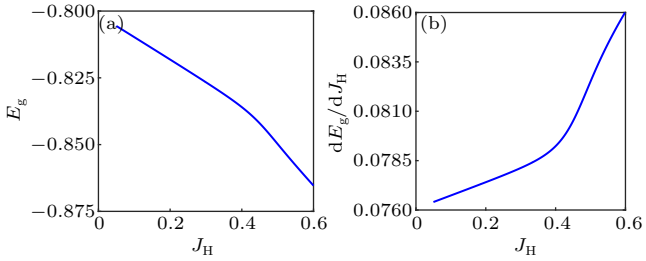


Fig. 6. (a) The ground-state energy $E_{\rm g}$ and (b) the first derivative $\mathrm{d}E_{\rm g}/\mathrm{d}J_{\rm H}$ versus the Heisenberg interaction $J_{\rm H}$ for NN electron hopping but with NNN hole hopping, where the parameters are $t = 1$, $t_1/t = 0.3$, $n_{\rm c} = 0.9$, $J_{\rm K} = 2.5$.

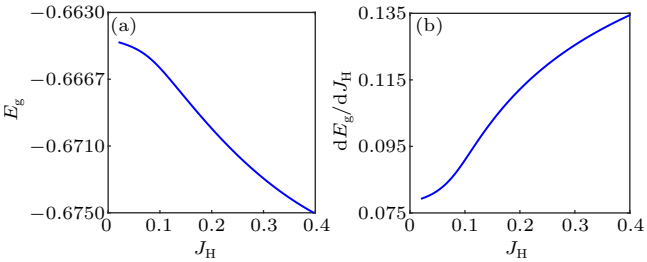


Fig. 7. (a) The ground-state energy $E_{\rm g}$ and (b) the first derivative $\mathrm{d}E_{\rm g}/\mathrm{d}J_{\rm H}$ versus the Heisenberg interaction $J_{\rm H}$ for NN hole hopping but with NNN electron hopping, where the parameters are $t = -1$, $t_1/t = 0.3$, $n_{\rm c} = 0.9$, $J_{\rm K} = 2.5$.

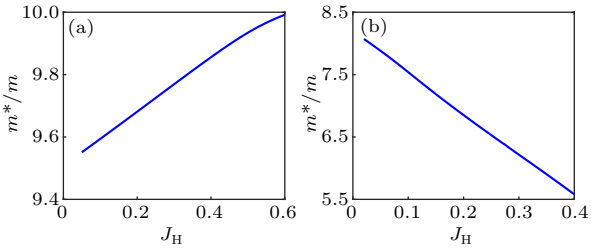


Fig. 8. The effective mass enhancement $m^{\star}/m$ versus the Heisenberg coupling $J_{\rm H}$. Panel (a) is for NN electron hopping but with NNN hole hopping, where the parameters are $t = 1$, $t_1/t = 0.3$, $n_{\rm c} = 0.9$, $J_{\rm K} = 2.5$. Panel (b) is for NN hole hopping but with NNN electron hopping, where the parameters are $t = -1$, $t_1/t = 0.3$, $n_{\rm c} = 0.9$, $J_{\rm K} = 2.5$.

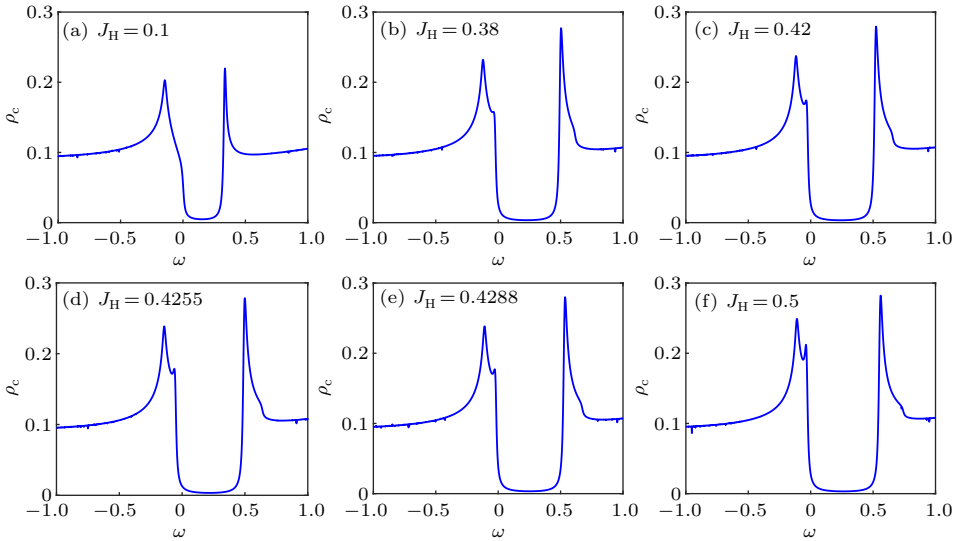


Fig. 9. The conduction electron DOS $\rho_{\rm c}$ for the KHM versus the Heisenberg interaction $J_{\rm H}$ for NN electron hopping but with NNN hole hopping, where the parameters are $t = 1$, $t_1/t = 0.3$, $n_{\rm c} = 0.9$, $J_{\rm K} = 2.5$. It is shown that the conduction electron DOS is changed after the Lifshitz transition.

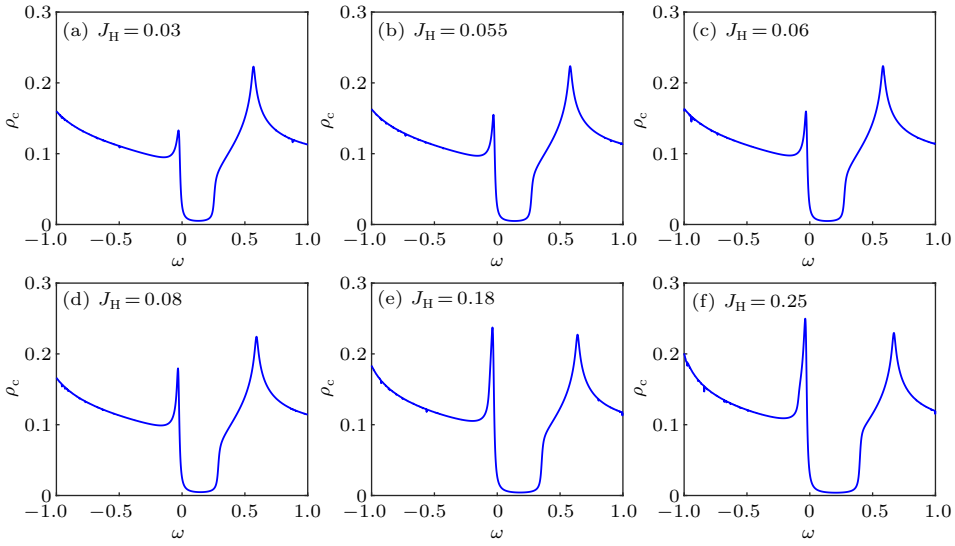


Fig. 10. The DOS of the conduction electron ρ_c for the KHM versus the Heisenberg interaction J_H for NN hole hopping but with NNN electron hopping, where the parameters are $t = -1$, $t_1/t = 0.3$, $n_c = 0.9$, $J_K = 2.5$. It is shown that the conduction electron DOS is changed after the Lifshitz transition.

Therefore, under the MF method,[23,49] when Heisenberg superexchange J_H increases, the presence of the short-range antiferromagnetic correlation gradually changes the electronic structure, and leads to the mentioned two kinds of Lifshitz transitions, which is similar to Ref. [23]. However, our work finds the continuous transition around the Lifshitz transition, which is different from that in the square lattice, i.e., the first-order and second-order phase transitions.[23]

With the FS topology of the quasiparticles changed, the area of FS varies at some critical values. To get more insight into the Lifshitz transition, it is helpful to use an effective low-energy theory to grasp the basic physical feature. Since the Lifshitz transition is mainly a single particle problem, one may use the following simple action:

$$S = \int \mathrm{d}\tau \mathrm{d}^2x \left[\psi^\dagger \left(\partial_\tau - \frac{\nabla^2}{2M} - r \right) \psi \right], \tag{11}$$

where M and r denote the effective mass and the effective chemical potential, respectively. The fermionic field ψ represents the fermions whose FS will vanish (appear) when $r < 0$ ($r > 0$). Since the most radical effect of the Lifshitz transition is just such a disappearance/an appearance of FS due to some parameters like r here, we may expect that this action captures the nature of this transition. When $r < 0$, all fermions are gapped and no FS is observed, while there exists a notable FS if $r > 0$. At the transition point where $r = 0$, the FS reduces to a point and the corresponding local DOS is a constant. The specific heat at the transition point is $C_v \sim T$, which is undistinguished with the usual Fermi liquid's result.

We should note that the change of the FS topology, i.e., the Lifshitz transition, has a direct experimental implication. The Hall coefficient will change its sign when the electronic FS transforms into the hole-type one or some parts of FS disappear. Besides this, one can use the quantum oscillation to measure the effective mass of the quasi-particle as the signal of the Lifshitz transitions discussed here.

4. The differential conductance

The STM spectrum is one of the indispensable tools in the study of correlated quantum matter, especially for several quantum critical heavy-electron compounds, which is a real-space probe that measures a local conductance.[51–53] In the linear-response regime, the current–voltage characteristics is related to the local DOS of the material.[54] There are also many STM experiments on the heavy-fermion compounds like $YbRh_2Si_2$ and $CeCoIn_5$.[22,43,55–58] Those results coincide with angle-resolved photoemission spectroscopy to understand the physics of quantum critical point in heavy-fermion compounds.[53]

Here, we follow Ref. [50] to get the differential conductance $\mathrm{d}I(V)/\mathrm{d}V$ on the triangular lattice by

$$\frac{\mathrm{d}I(V)}{\mathrm{d}V} = t_c^2 N_{cc}(V) + t_f^2 N_{ff}(V) + 2t_c t_f N_{cf}(V), \tag{12}$$

where t_c is the tunneling amplitude of the conduction electron and t_f is for the f-electron. $N_{cc} = -\frac{1}{\pi}\mathrm{Im}G_{cc}$ is the DOS of conduction electron while $N_{ff} = -\frac{1}{\pi}\mathrm{Im}G_{ff}$ is for f-electron and their mixture is $N_{cf} = -\frac{1}{\pi}\mathrm{Im}G_{cf}$. $G_{cc}(\tau) = -\langle T_\tau c_{k\sigma}(\tau) c^\dagger_{k\sigma}(0)\rangle$ is the Green's function of the conduction electron, $G_{ff}(\tau) = -\langle T_\tau f_{k\sigma}(\tau) f^\dagger_{k\sigma}(0)\rangle$ is for f-electron, and $G_{cf}(\tau) = -\langle T_\tau c_{k\sigma}(\tau) f^\dagger_{k\sigma}(0)\rangle$ describes the many-body effects arising from the hybridization of the conduction band with the f-electron level.

To calculate DOS, it is helpful to introduce fermionic quasiparticles $A_{k\sigma}$ and $B_{k\sigma}$ with the following transformation:

$$f_{k\sigma} = v_k A_{k\sigma} + u_k B_{k\sigma}, \tag{13}$$

$$c_{k\sigma} = u_k A_{k\sigma} - v_k B_{k\sigma}, \tag{14}$$

where $u_k^2 = \frac{1}{2} + \frac{-\chi_k+(\varepsilon_k-\mu)}{2\sqrt{(\varepsilon_k-\mu-\chi_k)^2+(J_K V)^2}}$, $v_k^2 = 1-\mu_k^2$, and $u_k v_k = \frac{J_K V}{2\sqrt{(\varepsilon_k-\mu-\chi_k)^2+(J_K V)^2}}$. The energy spectrum is given by Eq. (3). Figure 11 shows the shape-lines of the differential conductance $\mathrm{d}I/\mathrm{d}V$ in NN electron hopping with NNN hole hopping, and figure 12 shows the case of NN hole hopping with NNN electron hopping. With increasing the ratio of amplitudes t_f/t_c, the hybridization between the conduction electron band and f-electron band is different.

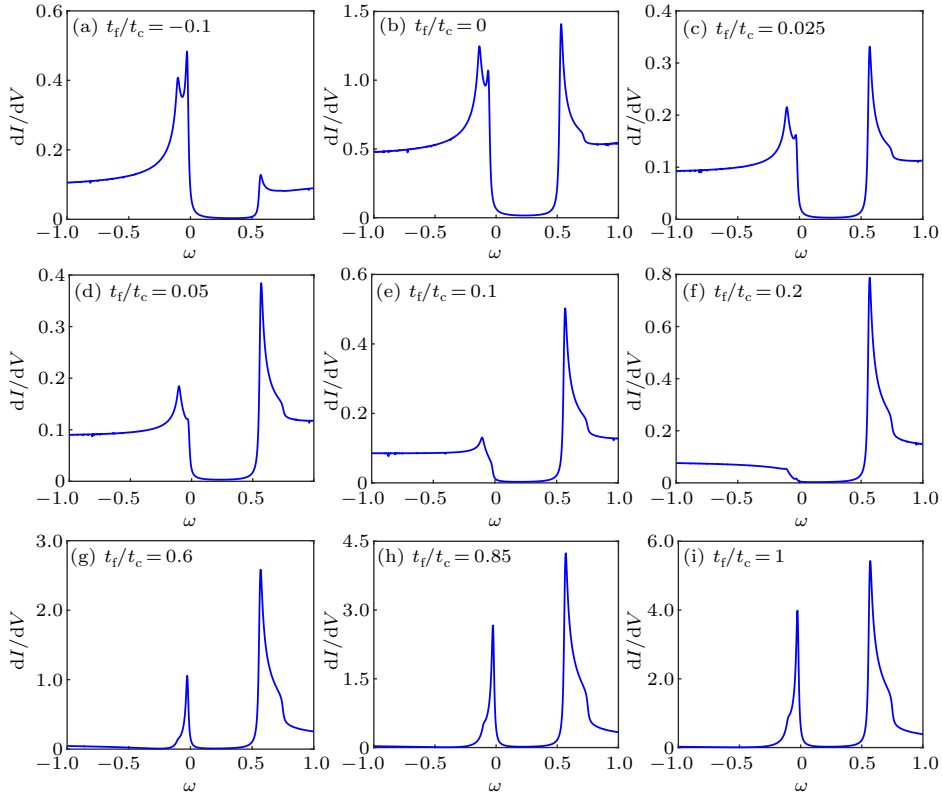


Fig. 11. The STM spectra of the KHM versus the ratio of amplitudes t_f/t_c for NN electron hopping but with NNN hole hopping, where the parameters are $t = 1$, $t_1/t = 0.3$, $n_c = 0.9$, $J_K = 2.5$. The ratio of amplitudes t_f/t_c influences the line-shape of the $\mathrm{d}I/\mathrm{d}V$.

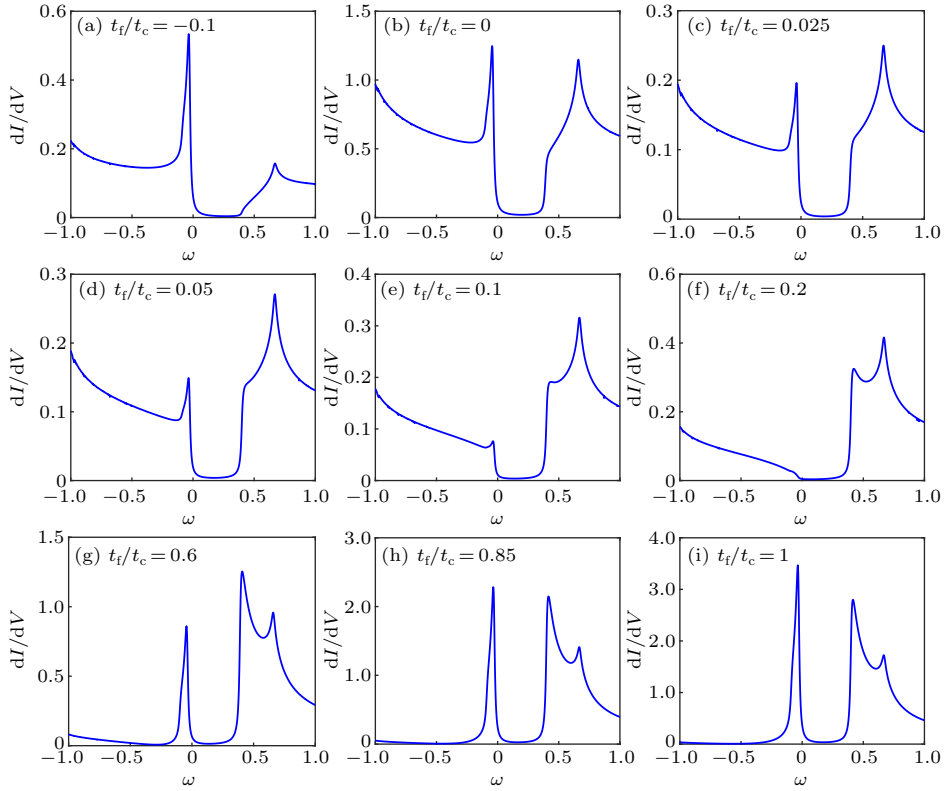


Fig. 12. The STM spectra of the KHM versus the ratio of amplitudes t_f/t_c for NN hole hopping but with NNN electron hopping, where the parameters are $t = -1$, $t_1/t = 0.3$, $n_c = 0.9$, $J_K = 2.5$. The ratio of amplitudes t_f/t_c influences the line-shape of the $\mathrm{d}I/\mathrm{d}V$.

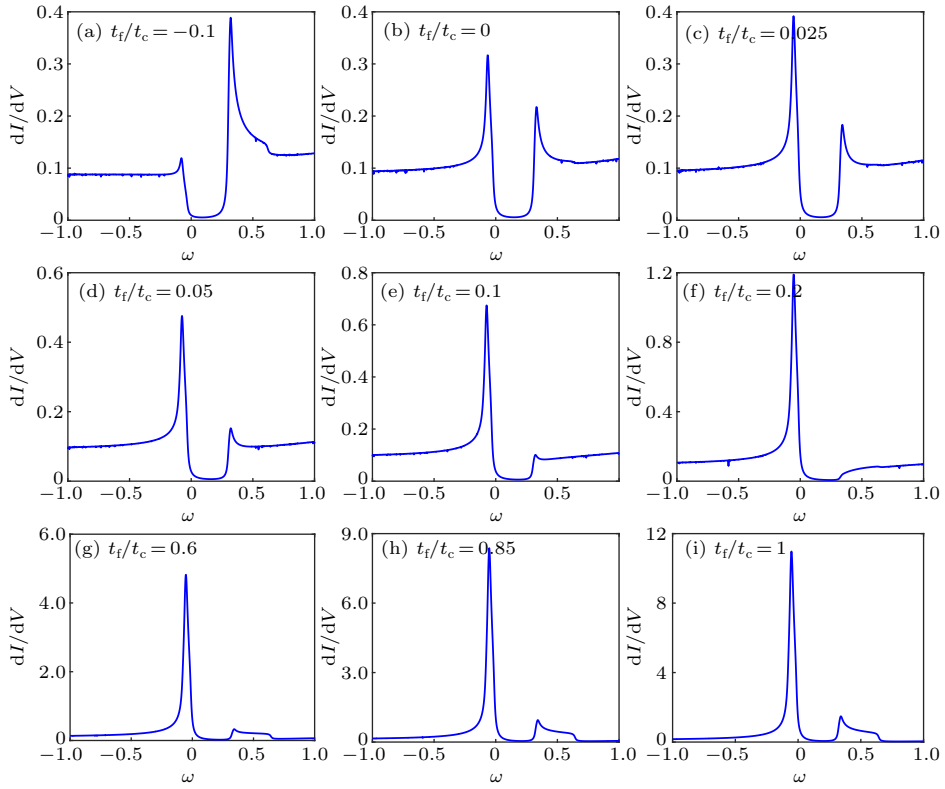


Fig. 13. The STM spectra of the KHM versus the ratio of amplitudes t_f/t_c for NN electron hopping but with NNN hole hopping, where the parameters are $t = 1$, $t_1/t = 0.3$, $n_c = 0.9$, $J_K = 2$. The ratio of amplitudes t_f/t_c influences the shape-line of the dI/dV.

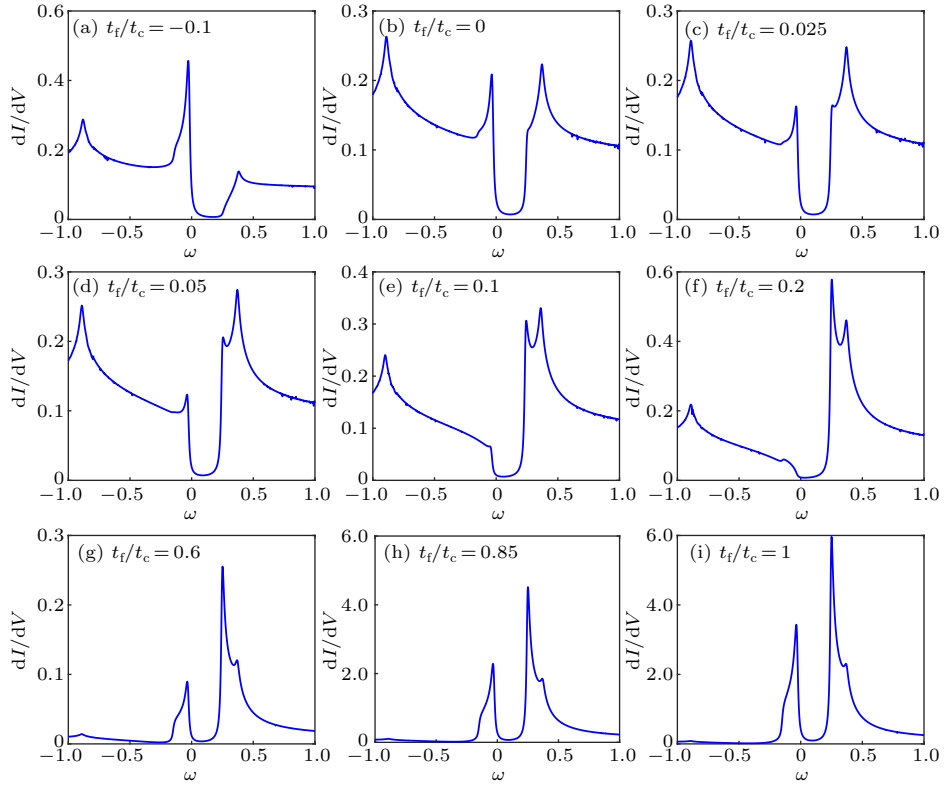


Fig. 14. The STM spectra of the KHM model versus the ratio of amplitudes t_f/t_c for NN hole hopping but with NNN electron hopping, where the parameters are $t = -1$, $t_1/t = 0.3$, $n_c = 0.9$, $J_K = 2$. The ratio of amplitudes t_f/t_c influences the shape-line of the dI/dV.

When increasing t_f/t_c, the line-shape changes quickly. Figures 11(a)–11(c) have three peaks and figures 11(h)–11(i) have two peaks. There emerges a peak when $\omega > 0$, and the peak is increasing versus t_f/t_c, which is the precursor of the emerging f-electron band.[50] Figures 12(a)–12(d) have two peaks and figures 12(h)–12(i) show three peaks. Figure 11(e) becomes two peaks while figure 12(e) begins to have three peaks. In Figs. 11(f) and 12(f), the left resonance peak nearly

vanishes, which means the suppression of the differential conductance around the Fermi energy.[50]

We also give the STM spectra of the different Kondo coupling J_K as shown in Figs. 13 and 14. Compared with Figs. 11 and 12, the line-shape varies versus t_f/t_c. There also exists the suppression of the differential conductance around the Fermi energy as shown in Figs. 13(e) and 14(e). Figures 11(b), 12(b), 13(b), and 14(b) are the DOS of the conduction electron.

Among these figures, the gap is increasing against the Heisenberg coupling J_H and the Kondo coupling J_K. The STM line-shape of the differential conductance dI/dV is mainly influenced by the ratio t_f/t_c in which the f-electron component becomes more and more significant. We also find that these spectra are qualitatively similar with those of $CeCoIn_5$.[43] These results show the existence of two resonance peaks structure in differential conductance as Refs. [50,59], which gives the insight to the heavy-fermion compounds by STM to examine the correlated electrons with high energy and spatial resolutions.[43]

5. Conclusion and perspective

In summary, we have investigated the KHM on triangular lattice with the fermionic large-N mean-field theory at the case of the NN electron hopping with NNN hole hopping and the case of the NN hole hopping and NNN electron hopping. At the heavy-fermion liquid state, the Heisenberg antiferromagnetic interaction (J_H) induces twice FS topology changes, i.e., the Lifshitz transition, where goes through the continuous quantum phase transition. In two cases, the conduction electron DOS is changed after the Lifshitz transition, the gap is influenced by the Kondo coupling J_K and the Heisenberg interaction J_H. The line-shape of the differential conductance dI/dV shows that the existence of two resonance peaks structure in differential conductance as in Refs. [50,59]. The short-range antiferromagnetic correlation coupling J_H, the ratio of the amplitudes of the f-electron to the amplitude of the the conduction electron t_f/t_c, and the Kondo correlation J_K influence the shape-line of the differential conductance dI/dV, which gives the insight to detect the heavy-fermion compounds STM spectra for examining the correlated electrons with high energy and spatial resolutions.[43]

As some triangular heavy-fermion compounds like YbAgGe[37–40] and $YbAl_3C_3$[41,42] have been found, we expect that our results may be confirmed by many FS measurements (Hall coefficient, de Haas–van Alphen measurements, angle-resolved photoemission spectroscopy, quasiparticle interference, and STM spectrum experiments) in those compounds.

Acknowledgements

This work was initially projected by Yu-Feng Wang, and most of it has been finished by authors listed here. The authors acknowledge useful result given by Wang.

References

[1] Lifshitz I 1960 *Sov. Phys. JETP* **11** 1130
[2] Norman M R, Lin J and Millis A J 2010 *Phys. Rev. B* **81** 180513
[3] Benhabib S, Sacuto A, Civelli M, Paul I, Cazayous M, Gallais Y, Measson M A , Zhong R D, Schneeloch J, Gu G D, Colson D and Forget A 2015 *Phys. Rev. Lett.* **114** 147001
[4] LeBoeuf D, Doiron-Leyraud N, Vignolle B, Sutherland M, Ramshaw B J, Levallois J, Daou R, Laliberté F, Cyr-Choinière O, Chang J, Jo Y J, Balicas L, Liang R, Bonn D A, Hardy W N, Proust C and Taillefer L 2011 *Phys. Rev. B* **83** 054506
[5] Khan S N and Johnson D D 2014 *Phys. Rev. Lett.* **112** 156401
[6] Hodovanets H, Liu Y, Jesche A, Ran S, Mun E D, Lograsso T A, Bud'ko S L and Canfield P C 2014 *Phys. Rev. B* **89** 224517
[7] Cho K, Konczykowski M, Teknowijoyo S, Tanatar M A, Liu Y, Lograsso T A, Straszheim W E, Mishra V, Maiti S, Hirschfeld P J and Prozorov R 2016 *Sci. Adv.* **2** e1600807
[8] Liu Y and Lograsso T A 2014 *Phys. Rev. B* **90** 224508
[9] Sato T, Nakayama K, Sekiba Y, Richard P, Xu Y M , Souma S, Takahashi T, Chen G F, Luo J L, Wang N L and Ding H 2009 *Phys. Rev. Lett.* **103** 047002
[10] Nakayama K, Sato T, Richard P, Xu Y M , Kawahara T, Umezawa K, Qian T, Neupane M, Chen G F, Ding H and Takahashi T 2011 *Phys. Rev. B* **83** 020501
[11] Malaeb W, Shimojima T, Ishida Y, Okazaki K, Ota Y, Ohgushi K, Kihou K, Saito T, Lee C H, Ishida S, Nakajima M, Uchida S, Fukazawa H, Kohori Y, Iyo A, Eisaki H, Chen C T , Watanabe S, Ikeda H and Shin S 2012 *Phys. Rev. B* **86** 165117
[12] Xu N, Richard P, Shi X, van Roekeghem A, Qian T, Razzoli E, Rienks E, Chen G F , Ieki E, Nakayama K, Sato T, Takahashi T, Shi M and Ding H 2013 *Phys. Rev. B* **88** 220508
[13] Liu C, Kondo T, Fernandes R M, Palczewski A D, Mun E D, Ni N, Thaler A N, Bostwick A, Rotenberg E, Schmalian J, Budko S L, Canfield P C and Kaminski A 2010 *Nat. Phys.* **6** 419
[14] Volovik G 2017 *Low Temperature Physics* **43** 47
[15] Iorsh I V, Dini K, Kibis O V and Shelykh I A 2017 *Phys. Rev. B* **96** 155432
[16] Daou R, Bergemann C and Julian S R 2006 *Phys. Rev. Lett.* **96** 026401
[17] Harrison N, Sebastian S E, Mielke C H, Paris A, Gordon M J, Swenson C A, Rickel D G, Pacheco M D, Ruminer P F, Schillig J B, Sims J R, Lacerda A H, Suzuki M T, Harima H and Ebihara T 2007 *Phys. Rev. Lett.* **99** 056401
[18] Purcell K M, Graf D, Kano M, Bourg J, Palm E C, Murphy T, McDonald R, Mielke C H, Altarawneh M M, Petrovic C, Hu R, Ebihara T, Cooley J, Schlottmann P and Tozer S W 2009 *Phys. Rev. B* **79** 214428
[19] Schlottmann P 2011 *Phys. Rev. B* **83** 115133
[20] Pfau H, Daou R, Lausberg S, Naren H R, Brando M, Friedemann S, Wirth S, Westerkamp T, Stockert U, Gegenwart P, Krellner C, Geibel C, Zwicknagl G and Steglich F 2013 *Phys. Rev. Lett.* **110** 256403
[21] Aoki D, Seyfarth G, Pourret A, Gourgout A, Mc-Collam A, Bruin J A N, Krupko Y and Sheikin I 2016 *Phys. Rev. Lett.* **116** 037202
[22] Paschen S, Lühmann T, Wirth S, Gegenwart P, Trovarelli O, Geibel C, Steglich F, Coleman P and Si Q 2004 *Nature* **432** 881
[23] Zhang G M , Su Y H and Yu L 2011 *Phys. Rev. B* **83** 033102
[24] Zhong Y, Zhang L, Lu H T and Luo H G 2015 *Eur. Phys. J. B* **88** 238
[25] Liu Y, Zhang G M and Lu Y 2014 *Chin. Phys. Lett.* **31** 087102
[26] Bercx M and Assaad F F 2012 *Phys. Rev. B* **86** 075108
[27] Nandy S, Mohanta N, Acharya S and Taraphder A 2016 *Phys. Rev. B* **94** 155103
[28] Burdin S and Lacroix C 2013 *Phys. Rev. Lett.* **110** 226403
[29] Grandi F, Amaricci A, Capone M and Fabrizio M 2018 *Phys. Rev. B* **98** 045105
[30] Sinha S K, Lander G H, Shapiro S M and Vogt O 1980 *Phys. Rev. Lett.* **45** 1028
[31] Zieba A, Slota M and Kucharczyk M 2000 *Phys. Rev. B* **61** 3435
[32] Isaev L and Vekhter I 2013 *Phys. Rev. Lett.* **110** 026403
[33] Hoshino S and Kuramoto Y 2013 *Phys. Rev. Lett.* **111** 026401
[34] Asadzadeh M Z, Becca F and Fabrizio M 2013 *Phys. Rev. B* **87** 205144
[35] Hackl A and Vojta M 2008 *Phys. Rev. B* **77** 134439
[36] Hackl A and Vojta M 2011 *Phys. Rev. Lett.* **106** 137002
[37] Bud'ko S L, Morosan E and Canfield P C 2005 *Phys. Rev. B* **71** 054408

[38] Dong J K, Tokiwa Y, Bud'ko S L, Canfield P C and Gegenwart P 2013 *Phys. Rev. Lett.* **110** 176402
[39] Bud'ko S L, Morosan E and Canfield P C 2004 *Phys. Rev. B* **69** 014415
[40] Tokiwa Y, Garst M, Gegenwart P, Bud'ko S L and Canfield P C 2013 *Phys. Rev. Lett.* **111** 116401
[41] Khalyavin D D, Adroja D T, Manuel P, Daoud-Aladine A, Kosaka M, Kondo K, McEwen K A, Pixley J H and Si Q 2013 *Phys. Rev. B* **87** 220406
[42] Hara K, Matsuda S, Matsuoka E, Tanigaki K, Ochiai A, Nakamura S, Nojima T and Katoh K 2012 *Phys. Rev. B* **85** 144416
[43] Aynajian P, da Silva Neto E H, Gyenis A, Baumbach R E, Thompson J, Fisk Z, Bauer E D and Yazdani A 2012 *Nature* **486** 201
[44] Coleman P and Andrei N 1989 *J. Phys.: Condens. Matter* **1** 4057
[45] Arispe J, Coqblin B and Lacroix C 1995 *Physica B* **206-207** 255
[46] Iglesias J R, Lacroix C, Arispe J and Coqblin B 1996 *Physica B* **223-224** 160
[47] Lacroix C, Iglesias J, Arispe J and Coqblin B 1997 *Physica B* **230–232** 503
[48] Read N and Newns D M 1983 *J. Phys. C: Solid State Phys.* **16** 3273
[49] Liu Y, Li H, Zhang G M and Yu L 2012 *Phys. Rev. B* **86** 024526
[50] Figgins J and Morr D K 2010 *Phys. Rev. Lett.* **104** 187202
[51] Damascelli A, Hussain Z and Shen Z X 2003 *Rev. Mod. Phys.* **75** 473
[52] Fischer O, Kugler M, Maggio-Aprile I, Berthod C and Renner C 2007 *Rev. Mod. Phys.* **79** 353
[53] Kirchner S, Paschen S, Chen Q, Wirth S, Feng D and Thompson J D and Si Q 2018 arXiv:Q1810.13293
[54] Tersoff J and Hamann D R 1985 *Phys. Rev. B* **31** 805
[55] Kummer K, Patil S, Chikina A, Güttler M, Hoppner M, Generalov A, Danzenbacher S, Seiro S, Hannaske A, Krellner C, Kucherenko Y, Shi M, Radovic M, Rienks E, Zwicknagl G, Matho K, Allen J W, Laubschat C, Geibel C and Vyalikh D V 2015 *Phys. Rev. X* **5** 011028
[56] Allan M, Massee F, Morr D, Van Dyke J, Rost A, Mackenzie A, Petrovic C and Davis J 2013 *Nat. Phys.* **9** 468
[57] Zhou B B, Misra S, da Silva Neto E H, Aynajian P, Baumbach R E, Thompson J, Bauer E D and Yazdani A 2013 *Nat. Phys.* **9** 474
[58] Thompson J D and Fisk Z 2012 *J. Phys. Soc. Jpn.* **81** 011002
[59] Maltseva M, Dzero M and Coleman P 2009 *Phys. Rev. Lett.* **103** 206402